

***K*-shell diagram and hypersatellite spectra of 4*d* transition elements**R. Diamant,¹ S. Huotari,² K. Hämäläinen,^{3,*} R. Sharon,¹ C. C. Kao,⁴ V. Honkimäki,² T. Buslaps,² and M. Deutsch¹¹*Department of Physics, Bar-Ilan University, Ramat-Gan 52900, Israel*²*ESRF, 6 rue Jules Horowitz, BP 220, F-38043 Grenoble cedex, France*³*Department of Physics, University of Helsinki, P.O. Box 64, FI-00014 Helsinki, Finland*⁴*NSLS, Brookhaven National Laboratory, Upton, New York 11973, USA*

(Received 15 December 2008; revised manuscript received 16 March 2009; published 25 June 2009)

The *K*-shell diagram ($K\alpha_{1,2}$ and $K\beta_{1,3}$) and hypersatellite (HS) ($K^h\alpha_{1,2}$) spectra of Y, Zr, Mo, and Pd have been measured with high energy-resolution using photoexcitation by 90 keV synchrotron radiation. Comparison of the measured and *ab initio* calculated HS spectra demonstrates the importance of quantum electrodynamical (QED) effects for the HS spectra. Phenomenological fits of the measured spectra by Voigt functions yield accurate values for the shift of the HS from the diagram lines, the splitting of the HS lines, and their intensity ratio. Good agreement with theory was found for all quantities except for the intensity ratio, which is dominated by the intermediacy of the coupling of the angular momenta. The observed deviations imply that our current understanding of the variation of the coupling scheme from *LS* to *jj* across the periodic table may require some revision.

DOI: 10.1103/PhysRevA.79.062512

PACS number(s): 32.30.Rj, 32.70.-n, 32.80.Fb

I. INTRODUCTION

In the preceding paper [1], denoted hereafter as I, we discuss the various important issues addressable through high-resolution measurements of hypersatellite (HS) spectra. These include intrashell electronic interactions, relativistic effects in these interactions, the role of the Breit interaction and of quantum electrodynamic (QED) effects in the atomic structure, the coupling of angular momenta within the atom, and more [2–4]. These and other fundamentals of the atomic structure, as well as the excitation and deexcitation dynamics of the atom, allow going beyond the frozen-atom, independent-electron, and sudden approximations that prevailed throughout most of 20th century. For many of these issues, the variation with atomic number *Z* of the quantities derived from the HS spectra is very important [3,5]. For example, the $K^h\alpha_1$ line is spin-flip forbidden in the *LS* coupling scheme but becomes increasingly allowed as the coupling becomes more intermediate with increasing *Z*. Thus, the intensity ratio of the two HS lines, $K^h\alpha_1$ and $K^h\alpha_2$, is the most sensitive experimental measure for the level of intermediacy of the coupling scheme. Another example are the Breit interaction and QED effects, the magnitudes of which are reflected in the splitting of the two HS lines, and their shift from the diagram lines [4,6]. Their contributions increase with an increasing *Z* not only absolutely but also relative to all other effects. Although it was argued that electron-electron interactions should become less important with an increasing *Z* since with higher atomic charge the electron-nucleus Coulomb interaction becomes stronger, Briand *et al.* [7] found that such interactions are in fact significant for two-electron ionization even for heavy atoms. Moreover, the interplay between relativity and electron-electron interactions becomes more pronounced in higher-*Z* atoms [8]. Thus, measurements of HS spectra for as high *Z* as possible seem to be of great scientific value.

In spite of their importance, HS measurements for $Z \sim 50$ are rather scarce. The HS spectra of 3*d* transition elements have been studied experimentally reasonably well (although mostly with low resolution, as discussed in I), starting with the seminal measurements of Briand *et al.* [9,10] and ending, for the present, with our preceding paper I. High-resolution measurements of HS spectra of the 4*d* elements are, however, much fewer. This is particularly true for studies employing the more controlled and less violent excitation methods by electrons and photons. These methods yield HS spectra free from contamination by higher-order spectra, which plague spectra excited by heavy-ion bombardment [11]. The main reason for the scarcity of high-resolution HS spectra for the 4*d* transition elements are the low cross sections for creating the initial two-*K*-hole state, $[1s]^{-2}$, of the HS transitions, $[1s]^{-2}(^1S_0) \rightarrow [1s2p]^{-1}(^{1,3}P_1)$. These cross sections are 10^{-4} – 10^{-5} times smaller than those of the $[1s]^{-1}$ initial state of the corresponding diagram lines. Furthermore, the cross section decreases as Z^{-4} .

The development of high-energy and high-intensity insertion device beamlines at third-generation synchrotrons made it possible to extend the high-resolution HS measurements discussed in I to higher-*Z* elements by providing high-intensity x-ray beams at energies ≥ 40 keV, required for exciting the HS spectra in the *Z* range discussed here. The availability of high-energy beams is a prerequisite for such measurements not only because of the high threshold energies, more than twice the binding energy of the *K* electrons, but also because of the extended energy range (well over 70% of the threshold energy) required for reaching the saturation intensity of the HS spectrum, as shown in I.

We present here the results of a high-resolution experimental study of the spectra of five elements from the 4*d* transition metals group, using photoexcitation by 90 keV x rays. The only experimental studies available for these elements were done by ion [11–14] and electron bombardment [15,16] with a single study (of Pd) using electron capture [17]. The ion-excited studies show a strong overlap by

*keijo.hamalainen@helsinki.fi

TABLE I. Experimental setup data for each of the samples. d , Anl, and ρ are, respectively, the sample's thickness, the analyzer, and its radius of curvature. The energies of the excitation threshold, $[1s]^{-2}$, and of the hypersatellite $K^h\alpha_2$ emission line are also listed. They were calculated using the $Z+1$ approximation [10], with energies taken from Bearden [37].

Sample	d (μm)	Anl (hkl)	ρ (m)	$K^h\alpha_2$ (keV)	$[1s]^{-2}$ (keV)
Y	250	Ge(220)	3.51	15.278	34.623
Zr	25	Si(111)	6.72	16.096	36.556
Mo	50	Si(111)	7.07	17.802	40.595
Pd	25	Si(111)	8.61	21.490	49.364
Sn	250	Si(111)	9.83	25.555	59.136

higher-order spectra. The low-resolution studies by Horvat *et al.* [14] and van Eijk *et al.* [17] did not resolve the two lines of the HS doublet. The sophisticated coincidence method used by Kanter *et al.* [18–20] for Mo and Ag HS measurements was able to provide accurate values for the cross section but not resolved HS spectra. The present measurements provide photoexcited doublet-resolved HS spectra for the elements studied, addressing a very sparsely studied, although important, Z interval of the periodic table.

The experimental techniques and data analysis methods, particularly aspects differing from those in I, are discussed in the next section, which is followed by a section presenting and discussing our results. The final section provides the conclusions of this study.

II. EXPERIMENT

A. Setup

Measurements were carried out at beamline ID15B at the European Synchrotron Radiation Facility (ESRF), Grenoble, France. The radiation from an asymmetric multipole wiggler was monochromatized by a horizontally focusing bent silicon monochromator using either the Si(111) or the Si(311) reflections in Bragg geometry, or the Si(511) in Laue geometry. Depending on the choice of the monochromator, fixed photon energies of 30, 60, or 90 keV were obtained. The HS and diagram spectra were recorded with an incident photon energy of 90 keV, where the photon flux was 2×10^{12} photons/s in a spot size of ~ 1 mm² on the sample. The incident photon flux was monitored with a Si *pin* diode placed in the beam upstream from the sample. The samples, which were foils of Y, Zr, Mo, Pd, and Sn (see Table I), were mounted in a lead-shielded vacuum chamber. The scattering angle was kept at 90°. Because of the 98% horizontal polarization of the beam, this reduced elastic, inelastic, and Compton scattering from the sample, thus minimizing the background. The angles of the incident and emitted radiations with respect to the sample's surface were typically 80° and 10°, respectively, in order to reduce the contribution of the source size to the spectrometer's resolution function.

The emission spectra were measured using a Johann-type scanning-crystal spectrometer in a Rowland circle geometry, described in detail in Ref. [21]. The analyzer crystal was a triangular Si(111) wafer [a Ge(220) in the case of Y], bent

cylindrically with a variable bending radius [22]. The bending radii used in measuring the spectra are summarized in Table I.

The detector employed was a liquid-nitrogen cooled intrinsic Ge detector, the relatively high energy-resolution of which helped to further minimize the background. Since this setup allowed us to measure the $K\alpha_{1,2}$ and $K\beta_{1,3}$ diagram lines along with the HS lines in a single scan, the energy scale could be calibrated to an accuracy well below 1 eV. This also allowed a direct and accurate measurement of the intensities of the HS spectra relative to those of the corresponding diagram spectra.

B. Line shape

A detrimental characteristic of the present setup is the skewed line shapes of the resolution function of the spectrometer resulting from the asymmetric reflectivity curve of the bent crystal. A typical example is shown in Fig. 1(a) for the $K\alpha_1$ line of Sn. The measured shape of the line (points) is very well approximated by the line shape calculated by a convolution of the resolution function, computed from the analyzer characteristics and spectrometer dimensions as detailed in Refs. [21,22], with the intrinsic Lorentzian emission line shape of a lifetime width of 11.2 eV [23]. The same procedure (with an intrinsic width of 5.7 eV) yields a good fit to the measured line shape of Zr in Fig. 1(b) only if the calculated resolution function is convoluted with a 4 eV wide Gaussian. This additional broadening could come from an imperfect bending (e.g., anticlastic bending or bending strains in the analyzer), a 10°–15° misalignment in the nominal 82° incidence angle on the sample, or both.

Figure 1(a) presents the worst case, i.e., the largest asymmetry, in our measurements. Note that the resolution full width at half height is ~ 47 eV, which is about fourfold the intrinsic Sn $K\alpha_1$ full width of 11.2 eV. Hence, the measured Sn $K\alpha_1$ line shape is dominated by the skewed resolution function. However, as discussed in I, the intrinsic width of a $K^h\alpha_1$ HS line is about threefold that of the diagram line [24]. This renders the resolution function only about 30–50% broader than the intrinsic Sn $K^h\alpha_1$ HS line. Thus, the domination of the resolution function is greatly reduced for the HS lines, and their shapes are considerably more symmetric than those of the diagram lines. In addition, the lower line

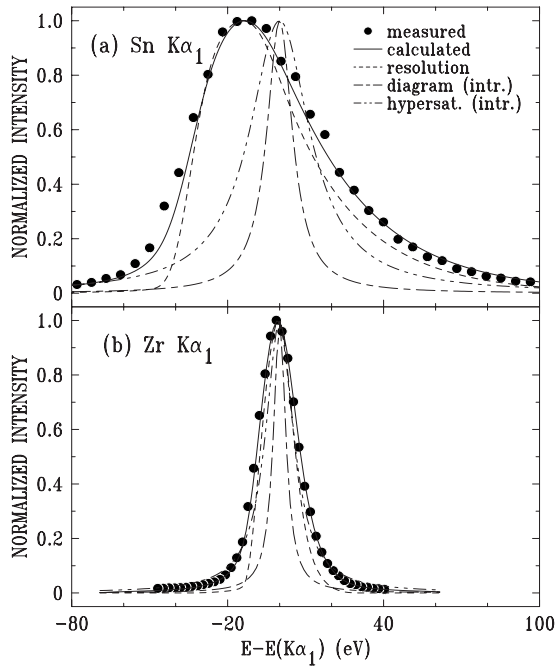


FIG. 1. (a) The measured (points) and calculated (solid line) Sn $K\alpha_1$ line. Note the skewed shape due to the asymmetric resolution function (dashed line). The theoretical intrinsic Lorentzian line shapes of the diagram $K\alpha_1$ and hypersatellite $K^h\alpha_1$ lines are also shown. (b) Same for Zr. Note the more symmetric line shape and smaller broadening due to the lower Z as discussed in the text.

energies, and consequently higher Bragg angles, of Y, Zr, Mo, and Pd, render the corresponding resolution functions more symmetric. This is observed in Fig. 1(b) for Zr, where the line shape is more symmetric. As can be observed in the figure, the intrinsic $K^h\alpha_1$ HS linewidth, 13 eV, is roughly equal in this case to that of the resolution function, introducing a negligible distortion to the HS line shapes, shown in Fig. 4.

C. Data analysis

1. Data correction

The measured spectra were corrected for absorption of the incident and emitted radiations within the sample and in the air path within the spectrometer, as well as for the dead time of the counting electronics as described in I and Refs. [22,25,26]. In addition, the spectra were corrected for the energy dependence of the integrated reflectivity of the analyzer, as calculated by the REFLECT code [21,22].

2. Phenomenological fit

Fits of spectra by analytic functions are common practice in spectroscopy. These are useful for calculating various physical quantities, which can be compared with results derived in previous measurements or calculations. For the intense high-statistics diagram lines, we used the Pearson VII function, P_{VII} [27]:

$$P_{VII}(E) = A \{ 1 + [(E - E_0)/\Gamma]^2/M \}^{-M}, \quad (1)$$

where A , E_0 , Γ , and M are, respectively, the amplitude, peak position, width, and a parameter controlling the decay of the

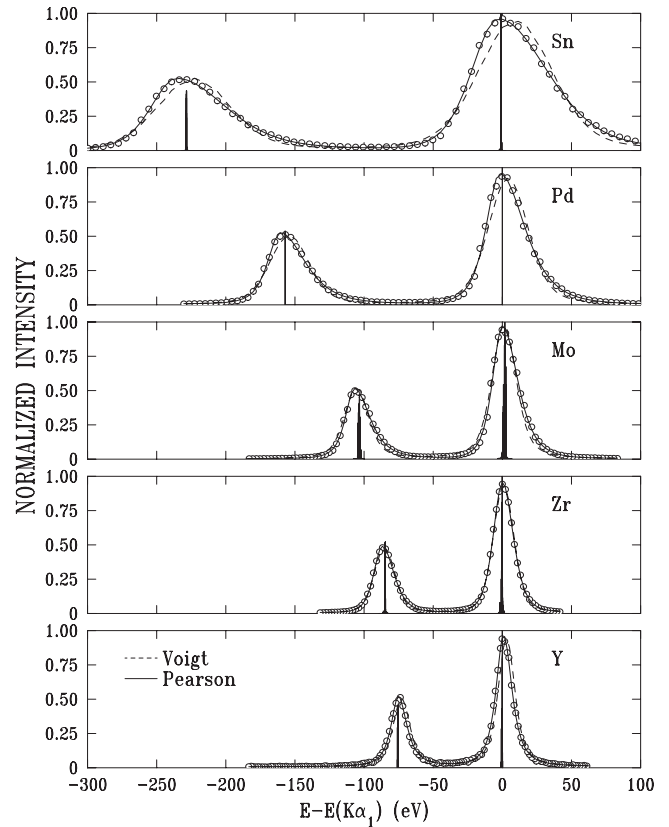


FIG. 2. Measured (circles) $K\alpha_{1,2}$ diagram lines, fitted phenomenologically with a single split Pearson VII (solid line) and Voigt (dashed line) functions per emission line. *Ab initio* RMCDF-calculated transition arrays normalized to the measured peaks are also shown.

tails, where $M=1$ yields a Lorentzian, and $M=\infty$ yields a Gaussian. For skewed lines the split version of Eq. (1) was used, with different widths and decay rates above and below the peak E_0 : Γ_-, M_- for $E < E_0$ and Γ_+, M_+ for $E > E_0$. Better fits were obtained using these functions than the Voigt functions used in I, as shown in Figs. 2 and 3. However, note that both figures demonstrate that the quality of the two fits becomes progressively closer as Z decreases due to the increasing symmetry of the measured spectral lines.

For the HS lines, where the counting statistics was considerably lower and the measured lines are more symmetric than the diagram lines, fits by P_{VII} and the simpler Voigt functions used in I yielded fits of equal quality. Thus, Voigt functions were used to fit the HS lines. The background underlying the HS lines, dominated by the tails of the diagram lines, was represented by the tails of two Lorentzians, centered on the diagram positions, and a linear term.

D. Fit to *ab initio* calculations

Relativistic multiconfigurational Dirac-Fock (RMCDF) transition arrays were calculated *ab initio* in the average level (AL) optimization mode for all spectra as described in I. For the diagram lines, these are shown as stick diagrams in Figs. 2 and 3. Note that, due to the high Z and consequent high energies, as compared to those of the $3d$ transition met-

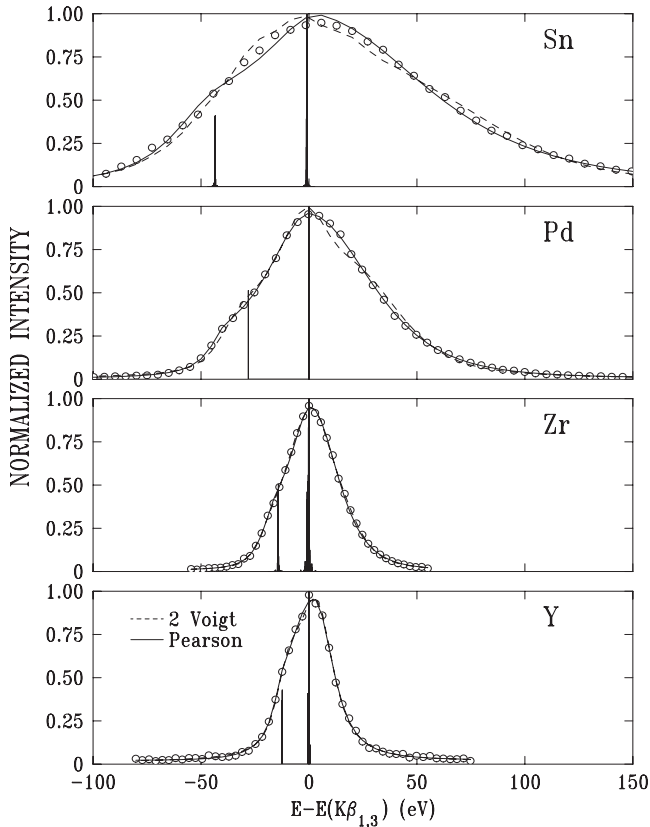


FIG. 3. Same as Fig. 2 but for the $K\beta_{1,3}$ spectra. The $K\beta_{1,3}$ spectrum of Mo was not measured.

als, the calculated sticks in Figs. 2 and 3 bunch strongly together into two narrow groups centered at the peaks of the two emission lines of the spectra. For example, the calculated fully split Mo $K\alpha_{1,2}$ spectrum consists of more than 28 000 sticks; yet all sticks of the $K\alpha_1$ line, about half this number, bunch within an interval of 2 eV. Thus, a fit employing such an array is very similar to a fit based on a single stick for each line, i.e., the phenomenological fit discussed in the previous section. Two well-separated bunches of the calculated doublet occur for the HS spectra as well, as shown in Fig. 4. This, in turn, allows a better *ab initio* calculation of the relative line intensities within each spectrum for both the diagram and the HS spectra than those of the $3d$ elements where the overlap between calculated sticks belonging to the two lines of each doublet is larger.

The measured HS spectra, shown in symbols in Fig. 4(a) for each element, were fitted by the RMCDF-calculated spectra, shown in Fig. 4(c), using a single Voigt function (VF) to represent each stick, as detailed above and in I. All VFs employ the same (fitted) width while the amplitude of each are set equal to the height of the corresponding stick. A single overall intensity parameter and a single experiment-theory shift are also refined in the fits. The fits, shown as solid lines in Fig. 4(a), are good, as indicated by the fact that the residuals in Fig. 4(b) are mostly within the $\pm 2\sigma$ lines of the measured points (σ is the standard deviation due to counting statistics in each point of the measured spectra). The experiment-theory shift obtained range from -0.3 eV for Pd to 4.7 eV for Y. Finally, the measurements of the Sn

HS spectra are more challenging than those of the other $4d$ elements measured here. First, the saturated cross section is intrinsically lower due to the Z^{-4} dependence mentioned above. The relative proximity of the threshold (59 keV) and incident (90 keV) energies further reduced the cross section due to the long saturation range of the HS's intensity, as discussed in I. The high HS energy, ~ 25 keV, render the Bragg angle, and the crystal's reflectivity, smaller than those of the other elements measured here. Thus the overall signal/background ratio for the Sn HS spectra was too unfavorable to allow measuring a useful HS spectrum within the limited time available at the synchrotron.

III. RESULTS AND DISCUSSION

A. Diagram lines

The $K\alpha_{1,2}$ and $K\beta_{1,3}$ diagram lines of all elements were fitted by a single split P_{VII} function for each line as discussed above. The resultant integrated intensity ratios $K\alpha_2/K\alpha_1$ and $K\beta_{1,3}/K\alpha_{1,2}$ are listed in Table II, along with those obtained in several previous studies, experimental and theoretical. The calculated $K\alpha_2/K\alpha_1$ intensity ratio of all elements agree to within $\lesssim 1.7\%$. The experimental results are spread over a significantly wider range. Nevertheless, all our measured values agree with the calculations within their experimental errors. Salem *et al.*'s [28] comprehensive evaluation of the then-available data (partially based on McCrary *et al.* [29], and Salem and Wimmer [30]) is also in good agreement with our results. The results of Herren and Dousse [31] for Mo and Pd are lower, and more accurate, than ours but still agree with our results within the combined experimental uncertainty.

For all but Sn, our measured $K\beta_{1,3}/K\alpha_{1,2}$ intensity ratios are higher than previous measurements but still within the combined error bars. For Sn, our value is lower than previous measurements although still within $1-2\sigma$. Several other measurements of the $K\beta/K\alpha$ intensity ratio [11,32–36] could not be compared with ours since they also include other spectral components, e.g., the $K\beta_{2,5}$ lines.

B. Hypersatellites

The phenomenological fits of the HS spectra by a single VF per line, as discussed above, are shown in Fig. 5. Within the admittedly larger error bars (as compared to those of the $3d$ transition-metal HS spectra shown in I) the fits are good. This is demonstrated by the fact that the residuals in panel (b) of each figure are almost all within the $\pm 2\sigma$ limits. The VFs were used to derive the shifts $\Delta_1 = E(K^h\alpha_1) - E(K\alpha_1)$ and $\Delta_2 = E(K^h\alpha_2) - E(K\alpha_2)$, the splitting $\delta = E(K^h\alpha_1) - E(K^h\alpha_2)$, and the intensity ratio $R = I(K^h\alpha_1)/I(K^h\alpha_2)$ listed in Table III, along with the same quantities obtained in earlier experimental and theoretical studies.

The present experimental and RMCDF-calculated shifts Δ_1 and Δ_2 mostly agree with each other. The exceptions are those of Mo, where both are upshifted by ~ 3 eV, and the Δ_1 of Pd, where a larger shift of ~ 5.5 eV is obtained. All theoretical studies agree with each other to within $\lesssim 1$ eV or

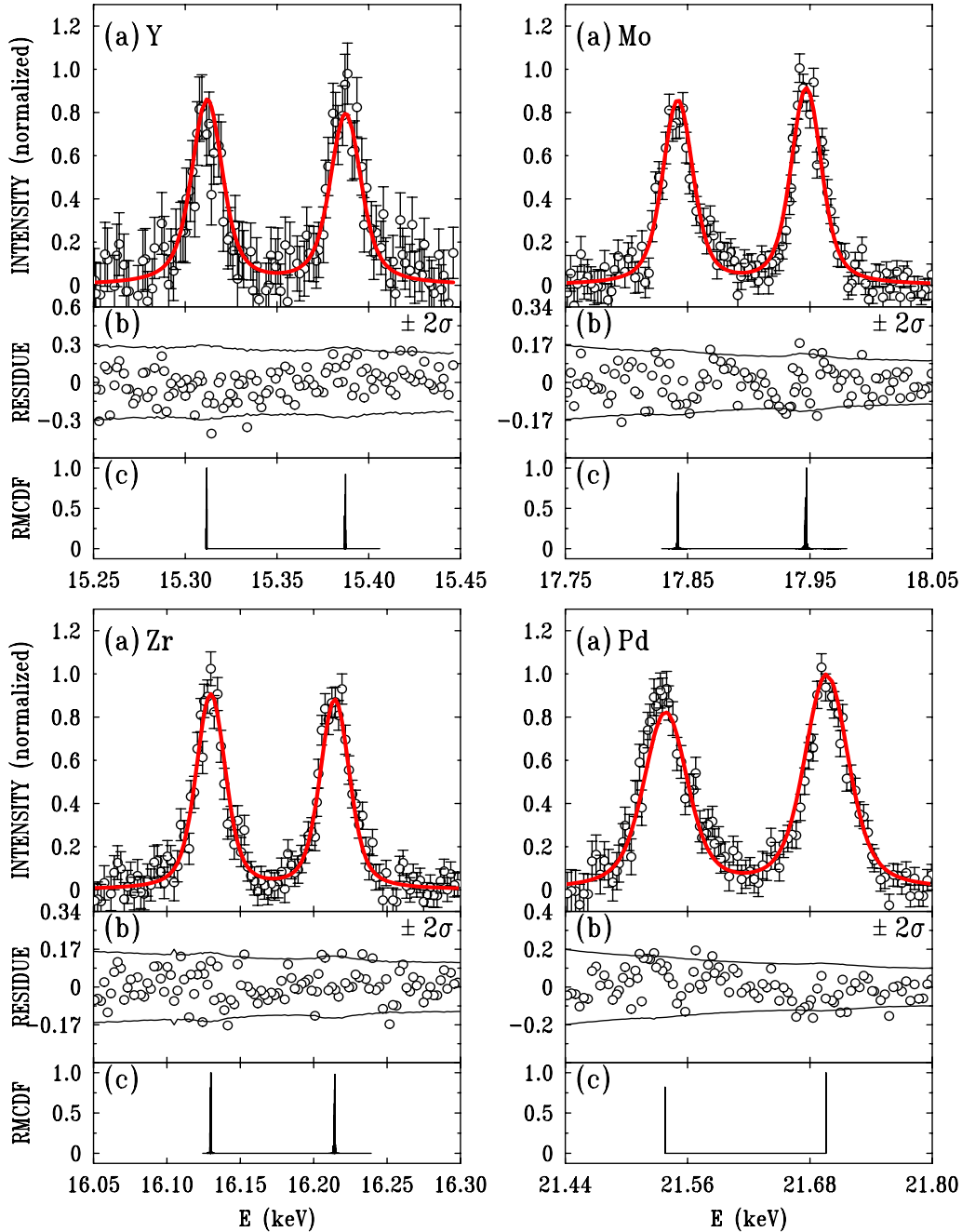


FIG. 4. (Color online) The $K^h\alpha_{1,2}$ hypersatellite spectra. (a) Measured (symbols) and fitted (lines) by the RMCDF-calculated spectra. (b) The residuals (symbols) and the $\pm 2\sigma$ boundaries (lines) of the fit. σ is the standard deviation in the measured values due to the counting statistics. The good quality of the fit is reflected in the residuals being mostly within the $\pm 2\sigma$ lines. (c) The *ab initio* RMCDF-calculated spectra.

better for all shifts except those of Åberg and Suvanén [6]. The values of Δ_1 of Natarajan [47] are lower than all other theoretical values, and underestimate the experimental values of both Mo and Pd by 5.2 and 7.6 eV, respectively. The fact that they neglect QED corrections and the Breit interaction in the mixing calculations is reflected in an upshift of a few eV for Δ_1 and a downshift of a few eV for Δ_2 relative to all other theoretical calculations and most experimental results.

The very few available experimental results listed in Table III, almost all ion excited, show a considerably larger scatter than the theoretical ones. The ion-excited measure-

ments of Boschung *et al.* [11], Rzadkiewicz *et al.* [12], and Rymuza *et al.* [13] are very close to the theoretical values. The electron-excited measurements of Salem *et al.* [15,16], available only for Mo and Zr, agree with ours and the ion-excited values albeit with a very large error bar of 8–9 eV. Their Δ_2 value for Zr shows an exceptional 16 eV deviation from all theoretical and experimental values but even this is less than two standard deviations. For Y, our shift values are the only experimental results available. They agree very well with our RMCDF and Chen *et al.*'s [4] Dirac-Hartree-Slater calculations. With this meager set of data, it is difficult to

TABLE II. Intensity ratios of the $K\alpha$ and $K\beta$ diagram spectra.

Sample	Source	$K\alpha_2/K\alpha_1$		$K\beta_{1,3}/K\alpha_{1,2}$	
		Experiment	Theory	Experiment	Theory
Y	Present ^a	0.548(34)	0.527	0.208(57)	
	Sc ^b		0.522		0.151
	SW ^c	0.523			
Zr	Present ^a	0.513(34)	0.529	0.184(57)	
	Sc ^b		0.523		0.153
	SW ^c	0.524			
	SPK ^d	0.523		0.166	
	M ^e	0.523(11)		0.163(7)	
	C ^f			0.1655(7)	0.1668
Mo	Present ^a	0.531(38)	0.532		
	Sc ^b		0.525		0.158
	SW ^c	0.525			
	SPK ^d	0.525		0.170	
	M ^e	0.528(11)		0.173(8)	
	C ^f			0.1698(7)	0.1718
	P ^g		0.525		
	HD ^h	0.514(5)			
Pd	Present ^a	0.536(39)	0.538	0.182(12)	
	Sc ^b		0.529		0.167
	SW ^c	0.526			
	SPK ^d	0.529		0.179	
	C ^f			0.1766(20)	0.1792
	P ^g		0.5297		
	HD ^h	0.528(5)			
	PL ⁱ	0.530(22)	0.53062		
Sn	Present ^a	0.557(29)	0.547	0.159(11)	
	Sc ^b		0.535		0.174
	SW ^c	0.541			
	SPK ^d	0.534		0.184	
	M ^e	0.531(11)		0.195(9)	
	C ^f			0.1843(40)	0.1850
	HD ^h	0.538(4)			

^aExperiment from P_{VII} fit. Theory from RMCDF calculation.

^bScofield [46]. Converted from $K\beta_1/K\alpha_1$.

^cSalem and Wimmer [30].

^dSalem *et al.* [28]. Converted from $K\beta/K\alpha$.

^eMcCrary *et al.* [29]. Converted from $K\beta_{1,3}/K\alpha_1$.

^fCampbell [42]. Converted from $K\beta_1/K\alpha_1$.

^gPolasik [43].

^hHerren and Dousse [31].

ⁱPolasik and Lewandowska-Robak [44].

asses how significant are the theory-experiment deviations in our shift results for Mo and Pd.

The line splitting δ shows an overall picture which is qualitatively similar to that of the shifts. As most authors report only the two shift values, the splittings listed in Table III were calculated by us from the reported shifts and the diagram line energies of Bearden [37]. All theoretical splittings agree with each other to better than 1 eV except those

of Åberg and Suvanén [6], where the shifts in $\Delta_{1,2}$ result in a few eV overestimation of all measured and calculated δ for all Z studied here. The splitting calculated by Natarajan [47] for Mo and Pd are the closest to our experimental values. The experimental values show again a considerably larger scatter, many outside their respective error bars. Our measured splittings are 1–2 eV larger than our theoretical values. The ion-excited results agree with theory for Mo and Pd but

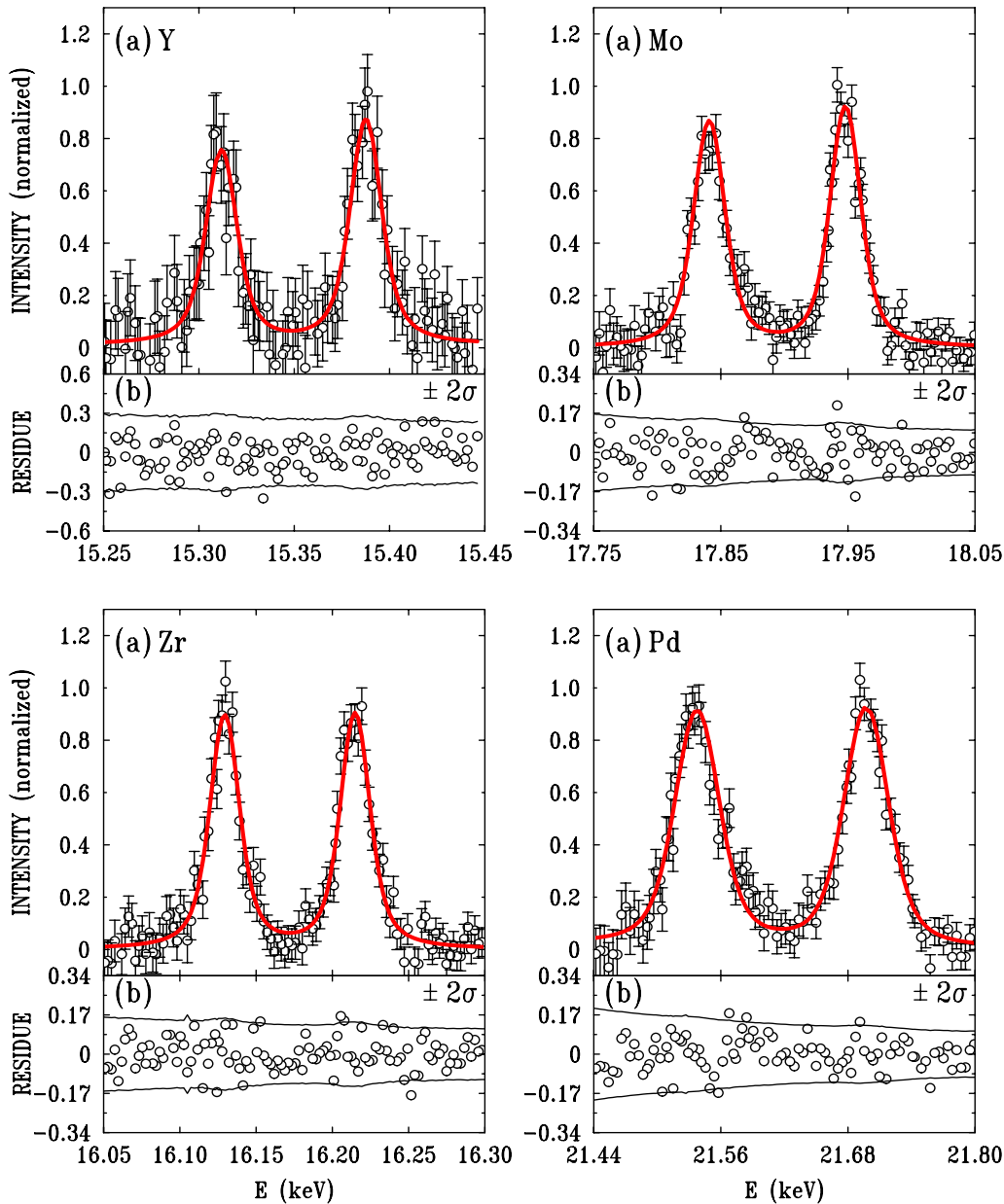


FIG. 5. (Color online) (a) Phenomenological fits (lines) of the measured $K^h\alpha_{1,2}$ hypersatellite spectra (symbols) by a single Voigt function per emission line. (b) The fit residuals (symbols) and the $\pm 2\sigma$ levels of the measurements (lines).

are lower by 1–2 eV than the theoretical values. The electron-excited measurements of Salem *et al.* [15,16] for Zr and Mo are lower by 20 and 7 eV, respectively, than the other measured and calculated values. However, the large error bars of Salem *et al.* [15,16] render these deviations a $<2\sigma$ effect only.

For the mid-Z atoms addressed here, the intermediate coupling scheme is already prominent, and thus, as discussed in I, the intensity ratio $R=I(K^h\alpha_1)/I(K^h\alpha_2)$ should start to exceed unity [10,45]. This is indeed observable in Fig. 6, particularly when compared to the corresponding Fig. 8 in I. Figure 6 also shows the strong (and nonlinear) increase in the line splitting δ with increasing Z , from 76 eV for Y to 160 eV for Pd. An examination of the values obtained for R shows, however, that our measured values are lower than the

theoretical predictions for the higher-Z Mo and Pd. The ion-excited measurements of Boschung *et al.* [11] yield R values which are consistently higher by 20–30% than ours and the theory. As discussed in Sec. I, this may be a result of the excitation mode, which does not allow a good control over the elimination of higher-order transitions. Indeed, the two extent electron-excitation values of Salem *et al.* [15,16] are closer to ours than those of Boschung *et al.* [11].

The Z dependence of the quantities discussed above are shown in Fig. 7, along with previous experimental results and two extensive theoretical calculations: the Dirac-Hartree-Slater results of Chen *et al.* [4], which take into consideration the Breit and QED effects fully, and the relativistic Dirac-Fock results of Åberg and Suvanen [6], which neglect them in the mixing calculations. Their exclusion of QED

TABLE III. Experimental and theoretical values of the HS spectra for the shifts Δ_1 and Δ_2 , the splitting δ , and the intensity ratio R , defined in the text.

Sample		Source	Δ_1	Δ_2	δ	R
Y	Experiment	Present ^a	425.6(8)	427.8(15)	75.7(6)	1.15(25)
		Theory	Present ^a	425.6	426.5	74.4
		CCM ^b	426.0	425.9	75.5 ^c	0.97
		AS ^d	427.6	423.8	79.4 ^c	0.96
Zr	Experiment	Present ^a	437.5(6)	438.5(12)	85.5(5)	1.03(7)
		B ^e	438.1(10)	438.9(10)	83.4(14) ^c	1.38(23)
		SK ^f	434.4(90)	454.5(90)	64(13) ^c	1.07(20)
		Rz ^g	439.0(3)	440.5(3)	82.7(4) ^c	1.07(11)
	Theory	Present ^a	438.6	438.6	84.5	0.97
		CCM ^b	438.9	439.0	84.2 ^c	1.03
		AS ^d	440.8	436.7	88.3 ^c	1.02
		B ^e	438.5	438.4	84.3 ^c	1.04
		Rz ^g	438.5	438.5	84.2 ^c	1.04
Mo	Experiment	Present ^a	468.0(4)	468.4(11)	107.1(5)	0.89(12)
		B ^e	465.2(10)	465.4(10)	104.8(14) ^c	1.34(19)
		Rz ^g	465.6(3)	465.6(3)	105.0(4) ^c	1.26(4)
		Ry ^h	465.5(4)	465.9(4)	104.6(6) ^c	1.23(6)
		S ⁱ	466.9(80)	473.9(80)	98(11) ^c	1.1(2)
		Theory	Present ^a	465.1	465.0	105.0
		CCM ^b	465.5	465.5	105.0 ^c	1.13
		AS ^d	467.7	463.1	109.6 ^c	1.12
		B ^e	463.7	464.3	104.4 ^c	1.14
		Rz ^g	465.0	464.9	105.1 ^c	1.14
		Ry ^h	465.0	464.92	105.1 ^c	1.161
		N ^k	462.8 ^l	464.1 ^l	106.3	1.14
Pd	Experiment	Present ^a	525.9(13)	519.8(16)	160.0(9)	0.96(15)
		B ^e	520.1(13)	519.8(19)	157.3(23) ^c	1.71(45)
		Rz ^g	520.3(4)	519.3(5)	158.0(6) ^c	1.13(5)
	Theory	Present ^a	520.4	519.6	157.9	1.22
		CCM ^b	520.9	520.3	157.6 ^c	1.31
		AS ^d	523.6	517.3	163.3 ^c	1.28
		B ^e	520.5	519.7	157.8 ^c	1.31
		Rz ^g	520.6	519.7	157.9 ^c	1.31
		Co ^j	520.01	519.14	158.01	1.32
		N ^k	518.3 ^l	520.1 ^l	158.8	1.32

^aExperiment from VF fit. Theory from RMCDF calculation.

^bChen *et al.* [4]. All results are interpolated except for given values of Mo.

^cCalculated as $\delta = (\Delta_1 - \Delta_2) + E(K\alpha_1) - E(K\alpha_2)$ with $E(K\alpha_1)$ and $E(K\alpha_2)$ taken from Ref. [37].

^dInterpolated from Åberg and Suvanén [6].

^eBoschung *et al.* [11].

^fSalem and Kumar [15].

^gRzadkiewicz *et al.* [12].

^hRymuza *et al.* [13].

ⁱSalem [16].

^jCosta *et al.* [39].

^kNatarajan [47].

^lCalculated as $\Delta_1 = E(K^h\alpha_1) - E(K\alpha_1)$ and $\Delta_2 = E(K^h\alpha_2) - E(K\alpha_2)$ with $E(K\alpha_1)$ and $E(K\alpha_2)$ taken from Ref. [37].

effects raises Δ_1 and lowers Δ_2 , and thus increases δ , as discussed above. Unfortunately, unlike the 3d transition metals discussed in I, the scatter in the available experimental results does not allow here a clear preference of one of the two calculation (Chen's and ours) over the other for δ and

Δ_2 . Thus, within the measurement accuracy of these two quantities, QED, Breit, and relativistic effects seem to be taken into account correctly by Chen *et al.*'s [4] and our calculations.

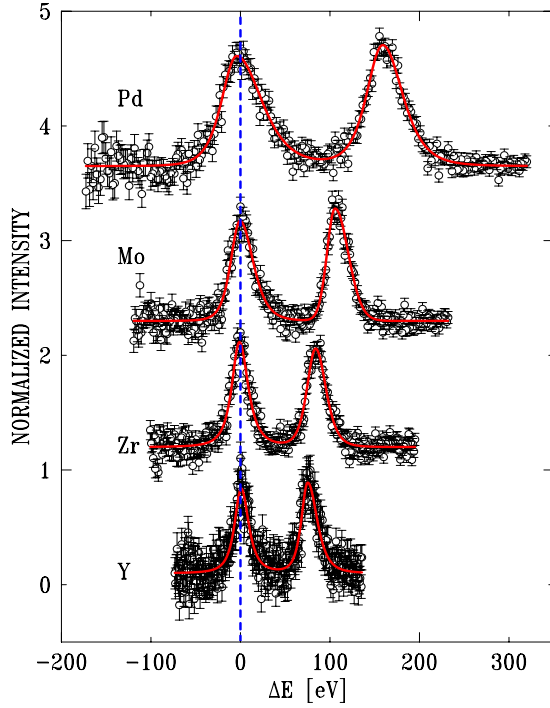


FIG. 6. (Color online) The measured (symbols) and phenomenologically fitted (lines) $K^h\alpha_{1,2}$ HS spectra for all elements studied. The intensity is normalized to unity at the $K^h\alpha_2$ peak of each spectrum. Spectra are vertically shifted for clarity by 1.1 each, and by 1.3 for Pd.

The values of R , however, exhibit a different trend. Here, the inclusion of the QED in the mixing calculations raises slightly the DHS values of Chen *et al.* [4] relative to the multiconfigurational Dirac-Fock (MCDF) values of Åberg and Suvanén [6] in this Z range. The positive contribution of QED effects and the Breit interaction contribution to R for $Z \geq 29$, a contribution being negative for $Z < 29$, have recently been demonstrated by the multiconfigurational Dirac-Fock calculations of Costa *et al.* [39]. Note, however, that the calculations of both Chen *et al.* [4] and Åberg and Suvanén [6] seem to overestimate our measured values. The improved wave functions provided by the GRASP package [38] used in our calculations provide a slightly better agreement with our measured R although still outside the error bars. The same trend of the theory overestimating the experimental R was also observed in I. Here, however, it is more prominent in spite of the larger error bars. These results hint that the intermediacy of the coupling, which dominates R , may require some modifications. We note that the limiting value reached by R at large Z differs considerably for the calculations of Chen *et al.* [4] and Åberg and Suvanén [6]. As shown in Fig. 8 in Ref. [4], the former predicts a maximum of $R \approx 1.66$ at $Z=72$, followed by a slow decrease. Costa *et al.* [39] calculate a very similar $R=1.65$ at $Z=80$. Åberg and Suvanén [6] predict a monotonically increasing R , reaching $R \approx 1.9$ at $Z=90$. Thus, the overall trend of Chen *et al.* [4] and Costa *et al.* [39] seems to agree better with our experimental results. Our *ab initio* calculations seem to indicate a somewhat lower maximal value for R , perhaps at a lower Z , further improving the agreement with our measurements.

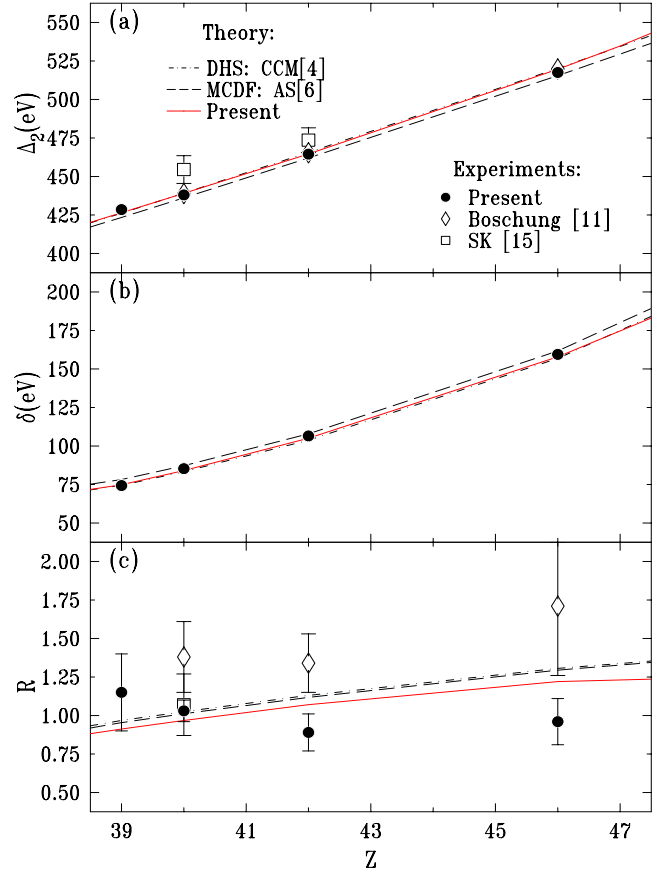


FIG. 7. (Color online) $K^h\alpha_{1,2}$ HS spectra characteristics. (a) HS-diagram energy shift $\Delta_2 = E(K^h\alpha_2) - E(K\alpha_2)$. (b) Line splitting $\delta = E(K^h\alpha_1) - E(K^h\alpha_2)$. (c) Integrated-intensity ratio of the two HS lines of each spectrum $R = I(K^h\alpha_1)/I(K^h\alpha_2)$. Numbers in square brackets indicate the corresponding references.

The verification of this speculation would require, however, more extensive calculations, which are outside the scope of the present paper. We note in passing that neglecting the Breit interaction in the DHS calculations of Chen *et al.* [4] leads also to a reduction in the maximal value reached by R to ~ 1.5 . This also lowers the calculated R values for the $4d$ transition elements, yielding a better agreement with our measured R . The R results for the lower- Z $3d$ transition elements discussed in I are hardly affected. The recent calculations of Costa *et al.* [39] demonstrate that the lower limiting value of R indeed survives when Dirac-Fock, rather than Dirac-Hartree-Slater, wave functions are used. Moreover, neglecting the Breit+QED contributions was shown by Costa *et al.* [39] to bring the limiting R value down to 1.59 for $Z=80$, and that of Pd down to 1.24, improving the agreement with our measured and calculated values. Clearly, calculations of the contributions of the individual QED effects, and a separation of the contribution of the Breit interaction, are required to better understand the evolution of the coupling in this Z range.

Figure 8 demonstrates the importance of the QED corrections for the HS spectra. As shown in Fig. 8(a) a good fit to the measured Pd HS spectrum is obtained with the RMCDF-calculated transition array (solid line), which includes these

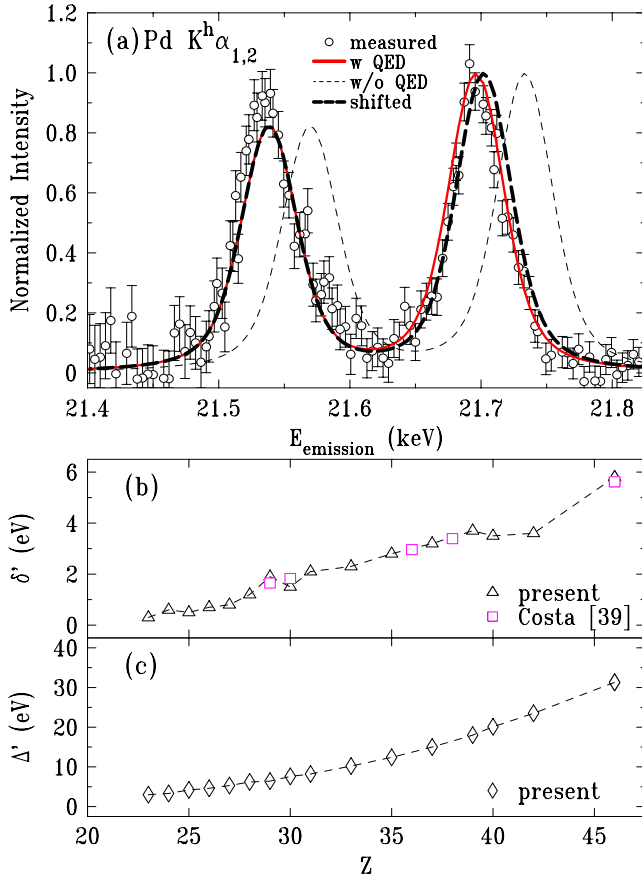


FIG. 8. (Color online) (a) A comparison of the measured Pd $K^h \alpha_{1,2}$ HS spectrum (symbols) with the RMCDF-calculated spectra with (solid line) and without (thin dashed line) QED corrections. The bold dashed line is the same as the light dashed line but downshifted to make the $K^h \alpha_2$ peak of the calculated and measured spectra coincide. (b) Z dependence of the difference in the line splittings, calculated without and with QED corrections, $\delta' = \delta^{-\text{QED}} - \delta^{+\text{QED}}$. (c) Z dependence of the difference in the shift of the $K^h \alpha_2$ line from the $K \alpha_2$ diagram line, calculated without and with QED corrections, $\Delta' = E^{-\text{QED}}(K^h \alpha_2) - E^{+\text{QED}}(K^h \alpha_2)$. For a discussion of these values in comparison to those of Costa *et al.* [39], see text.

corrections. However, when neglected, the calculations (thin dashed line) yield a 31 eV upshift in energy. Moreover, even downshifting the calculated spectrum by this large amount (bold dashed line) does not yield a satisfactory agreement with the measured spectrum due to its too large (by 6 eV) splitting. This additional splitting is considerably larger than the combined experimental errors in the positions of the two peaks. Similar results were obtained for Cu [25] and for Ni, as shown in Fig. 9 in I.

We have also calculated the Z dependence of the doublet splitting, δ , and the difference in the HS shift from the measured diagram line, Δ' , with and without QED correction using the RMCDF code GRASP of Dyall *et al.* [38]. Figure 8(b) demonstrates that neglecting the QED corrections results in a monotonic and roughly linear increase in δ with Z over the values obtained when the QED corrections are included, which are also very close to the measured values. The calculated δ' values of Costa *et al.* [39] agree closely

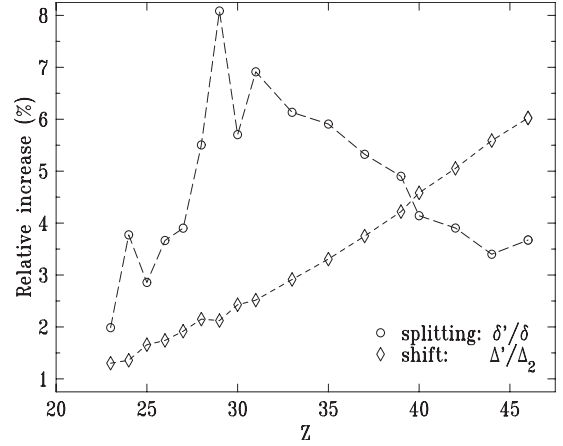


FIG. 9. The relative increase (in percents) of the splitting and shift due to neglecting the QED corrections in the *ab initio* calculation of the HS spectrum.

with ours, as shown in Fig. 8(b). A smoother, and roughly quadratic, increase is found for the difference in the shifts (calculated with and without QED corrections) of the HS lines from the diagram ones, Δ' , as shown in Fig. 8(c). It should be noted, however, that our HS shifts were calculated for both the “with QED” and the “without QED” cases relative to the measured diagram $K \alpha_2$ energies, which coincide with those calculated with QED. By contrast, Costa *et al.* [39] calculate their HS shifts for the without QED case from diagram line energies calculated also without QED corrections. Since the upshift of the without QED calculated *diagram* line energy (relative to the with QED one) exceeds considerably the upshift of the correspondingly calculated *hypersatellite* line energy, a net *downshift* is obtained for the HS line relative to the with QED case, yielding a negative Δ' shift difference with Costa *et al.*'s [39] method rather than the positive Δ' obtained with our different calculation method. Since Costa *et al.* [39] did not publish their calculated diagram and HS lines' absolute energies, only their relative shifts, a direct comparison of our calculated results with theirs is not possible. We have however calculated the with QED-without QED difference in the shift using their method (i.e., using, in the without QED case, diagram line energies also calculated without QED corrections) for Cu and Zn. For Cu we obtain 299 and 306 eV for the shift from the diagram lines calculated without and with QED corrections, respectively. These values coincide with those of Costa *et al.* [39]. For Zn we obtain 310 and 318 eV, respectively, while Costa *et al.* [39] obtain 309 and 317 eV. Thus, we conclude that our calculations agree well with those of Costa *et al.* [39] also for the HS lines' shifts from the diagram lines as calculated with and without QED corrections.

While our δ' and Δ' increase relatively smoothly and monotonically with Z over the $Z=23-46$ range explored in this and the accompanying [1] studies, the relative magnitudes δ'/δ and Δ'/Δ , shown in Fig. 9, reveal a nonmonotonic behavior for the former. For $23 \leq Z \leq 40$ δ'/δ is larger than Δ'/Δ by as much as a factor of 2 to 3. This supports the conclusion of Chen *et al.* [4] that δ is more sensitive to QED exclusion than Δ . However for $Z > 40$ the trend is reversed

and Δ'/Δ becomes up to twice as large as δ'/δ . This trend deserves a deeper theoretical investigation than that possible within the present experimental study.

IV. CONCLUSIONS

The results presented above provide resolved photoexcited x-ray $K^h\alpha_{1,2}$ hypersatellite spectra for all the elements studied here; some ion- and electron-excited resolved measurements already exist in the literature. The simultaneously measured $K\alpha_{1,2}$ diagram lines provide for a reliable calibration of the energy scale, the relative intensities, and the treatment of resolution effects which are very significant for the present measurement method. In addition to yielding fundamental phenomenological information on the spectra, such as line splitting, shift from the diagram lines, and the intensity ratios, the data allow a detailed comparison with *ab initio* theoretical calculations. This comparison reveals the continuation of trends observed already in I, namely, that current theoretical models of the atom account well for relativity, for QED effects, and for the Breit interaction, but less so for variation with Z of the coupling of the atomic angular momenta. The Breit contribution becomes particularly strong in the $39 \leq Z \leq 46$ region studied here. The intensity ratio R of the spectral lines, which best reflects the coupling behavior, is expected to peak in the $60 \leq Z \leq 75$ range. Measurements similar to the ones presented here in that range would therefore be very desirable for a better understanding of the coupling. In addition, energy-dependent measurements of the threshold behavior of the cross section for exciting these spectra would also be of interest. However, the fast decreasing cross section with increasing Z renders such measurements a very demanding task.

Looking at the study presented in the two papers as a whole, several questions remain unsolved and require further experimental and theoretical attention. Arguably, the most intriguing among these is the long saturation range of the excitation cross section of the hypersatellite spectra, discussed in I. On general principles this range should be commensurate with the binding energy of the nondirectly excited electron. Indeed, Huotari *et al.* [40] have recently demonstrated that, when scaled by this binding energy, the cross-section evolution curves of all $3d$ transition metals measured

in I collapse onto a single universal curve. However, a more fundamental theoretical description, going beyond these phenomenological observations, is called for to achieve a better understanding of the near-threshold evolution of the cross section. Moreover, the shape of the cross-section vs excitation energy curve does not agree with current theoretical understanding of the single-photon-two-electron excitation process as a shake up/off (SO) process. Among currently known processes, the direct classical knockout process (KO) seems to account much better for the near-threshold behavior although calculations are at present available only for He [41]. In those calculations, the classical nature of the KO process was employed to separate it from the quantum-mechanical SO process. When scaled phenomenologically to the appropriate energy range, the calculated KO curve of He was shown to agree well with the measured energy dependence of the measured double-to-single K -shell ionization cross-section ratio for both Ag [19,20], and the full set of scaled $3d$ transition elements [40]. However, to establish the dominance of the KO process from threshold to the cross section's maximum, it is mandatory to extend the Rost-type energy-dependent KO calculations to higher- Z elements rather than to use a phenomenological scaling. If the dominance of KO near threshold is indeed confirmed by future calculations, an intriguing situation may arise, whereby an inner-shell atomic process will be described as a classical, rather than a quantum-mechanical, effect, at least near threshold.

Note added in proof. The dominance of the KO process near threshold is also supported by the recent study of Hoszowska *et al.* [48] of the HS spectra of Mg, Al, and Si. That study demonstrates the importance of final-state electron-electron interactions, like those of the KO process, for double photoionization near threshold. It also exhibits a universal scaling behavior of the DPI cross section by the effective nuclear charge.

ACKNOWLEDGMENTS

Support by The Israel Science Foundation, Jerusalem (M.D.) and the Academy of Finland (Contracts No. 201291, 127462, and 205967 to K.H.), and beamtime at ID15B, ESRF, are gratefully acknowledged.

-
- [1] R. Diamant, S. Huotari, K. Hämäläinen, R. Sharon, C. C. Kao, and M. Deutsch, Phys. Rev. A **79**, 062511 (2009), the preceding paper.
- [2] J. P. Desclaux, Ch. Briançon, J. P. Thibaud, and R. J. Walen, Phys. Rev. Lett. **32**, 447 (1974).
- [3] B. Crasemann, in *Atomic Inner-Shell Physics*, edited by B. Crasemann, (Plenum, New York, 1986); B. Crasemann, M. H. Chen, and H. Mark, J. Opt. Soc. Am. B **1**, 224 (1984).
- [4] M. H. Chen, B. Crasemann, and H. Mark, Phys. Rev. A **25**, 391 (1982).
- [5] J. P. Desclaux, in *Proceedings of the 2nd International Conference on Inner Shell Ionization Phenomena*, edited by W. Mehlhorn and R. Brenn (Universität Freiburg, Freiburg, 1976), p. 351.
- [6] T. Åberg and M. Suvanen, in *Advances in X-Rays Spectroscopy*, edited by C. Bonnelle and C. Mande (Pergamon, New York, 1982).
- [7] J. P. Briand, P. Chevallier, A. Chetoui, J. P. Rozet, M. Tavernier, and A. Touati, Phys. Rev. A **23**, 39 (1981).
- [8] H. G. Berry, R. W. Dunford, and A. E. Livingston, Phys. Rev. A **47**, 698 (1993).
- [9] J. P. Briand, P. Chevallier, A. Touati, and J. P. Rozet, Phys. Rev. Lett. **27**, 777 (1971).
- [10] J. P. Briand, A. Touati, M. Frilley, P. Chevallier, A. Johnson, J.

- P. Rozet, M. Tavernier, S. Shafroth, and M. O. Krause, *J. Phys. B* **9**, 1055 (1976).
- [11] B. Boschung, J.-Cl. Dousse, B. Galley, Ch. Herren, J. Hozzowska, J. Kern, Ch. Rhême, Z. Halabuka, T. Ludziejewski, P. Rymuza, Z. Sujkowski, and M. Polasik, *Phys. Rev. A* **51**, 3650 (1995).
- [12] J. Rzadkiewicz, D. Chmielewska, T. Ludziejewski, P. Rymuza, Z. Sujkowski, D. Castella, D. Corminboeuf, J.-Cl. Dousse, B. Galley, Ch. Herren, J. Hozzowska, J. Kern, M. Polasik, and M. Pajek, *Phys. Lett. A* **264**, 186 (1999).
- [13] P. Rymuza, D. Chmielewska, T. Ludziejewski, Z. Sujkowski, D. Castella, D. Corminboeuf, J.-Cl. Dousse, B. Galley, Ch. Herren, J. Hozzowska, J. Kern, M. Polasik, and M. Pajek, in *Application of Accelerators in Research and Industry*, Proceedings of the 14th International Conference, AIP Conf. Proc. No. 392, edited by J. L. Dugan and I. L. Morgan (AIP, Melville, NY, 1997), p. 109.
- [14] V. Horvat, G. Sampoll, K. Wohrer, M. Chabot, and R. L. Watson, *Phys. Rev. A* **46**, 2572 (1992).
- [15] S. I. Salem and A. Kumar, *Phys. Rev. A* **28**, 2245 (1983).
- [16] S. I. Salem, *Phys. Rev. A* **21**, 858 (1980).
- [17] C. W. E. van Eijk, J. Wijnhorst, and M. A. Popelier, *Phys. Rev. C* **19**, 1047 (1979).
- [18] E. P. Kanter, R. W. Dunford, B. Krässig, and S. H. Southworth, *Phys. Rev. Lett.* **83**, 508 (1999); R. W. Dunford, E. P. Kanter, B. Krässig, S. H. Southworth, and L. Young, *Radiat. Phys. Chem.* **70**, 149 (2004).
- [19] E. P. Kanter, R. W. Dunford, B. Krässig, S. H. Southworth, and L. Young, *Radiat. Phys. Chem.* **75**, 2174 (2006).
- [20] E. P. Kanter, I. Ahmad, R. W. Dunford, D. S. Gemmell, B. Krässig, S. H. Southworth, and L. Young, *Phys. Rev. A* **73**, 022708 (2006).
- [21] P. Suortti, T. Buslaps, P. Fajardo, V. Honkimäki, M. Kretschmer, U. Lienert, J. E. McCarthy, M. Renier, A. Shukla, Th. Tschentscher, and T. Meinander, *J. Synchrotron Radiat.* **6**, 69 (1999).
- [22] P. Suortti, P. Pattison, and W. Weyrich, *J. Appl. Crystallogr.* **19**, 336 (1986); **19**, 343 (1986); E. Erola, V. Etelaniemi, P. Suortti, P. Pattison, and W. Thomlinson, *ibid.* **23**, 35 (1990).
- [23] S. I. Salem and P. L. Lee, *At. Data Nucl. Data Tables* **18**, 233 (1976).
- [24] J. P. Mossé, P. Chevallier, and J. P. Briand, *Z. Phys. A* **322**, 207 (1985).
- [25] R. Diamant, S. Huotari, K. Hämäläinen, C. C. Kao, and M. Deutsch, *Phys. Rev. Lett.* **84**, 3278 (2000); *Phys. Rev. A* **62**, 052519 (2000).
- [26] R. Diamant, S. Huotari, K. Hämäläinen, R. Sharon, C. C. Kao, and M. Deutsch, *Phys. Rev. Lett.* **91**, 193001 (2003).
- [27] H. Wang and J. Zhuo, *J. Appl. Crystallogr.* **38**, 830 (2005); L. Chen and M. Garland, *Appl. Spectrosc.* **57**, 331 (2003); J. I. Langford and D. Louër, *Rep. Prog. Phys.* **59**, 131 (1996).
- [28] S. I. Salem, S. L. Panossian, and R. A. Krause, *At. Data Nucl. Data Tables* **14**, 91 (1974).
- [29] J. H. McCrary *et al.*, *Phys. Rev. A* **4**, 1745 (1971).
- [30] S. I. Salem and R. J. Wimmer, *Phys. Rev. A* **2**, 1121 (1970).
- [31] Ch. Herren and J.-Cl. Dousse, *Phys. Rev. A* **56**, 2750 (1997).
- [32] P. V. Rao, M. H. Chen, and B. Crasemann, *Phys. Rev. A* **5**, 997 (1972).
- [33] M. I. Marques, M. C. Martins, and J. G. Ferreira, *J. Phys. B* **13**, 41 (1980).
- [34] I. Han, M. Şahin, L. Demir, and Y. Şahin, *Appl. Radiat. Isot.* **65**, 669 (2007).
- [35] U. Cevik, S. Kaya, B. Ertugral, H. Baltas, and S. M. Karabýdak, *Nucl. Instrum. Methods Phys. Res. B* **262**, 165 (2007).
- [36] B. B. Dhal and H. C. Padhi, *Phys. Rev. A* **50**, 1096 (1994).
- [37] J. A. Bearden, *Rev. Mod. Phys.* **39**, 78 (1967).
- [38] K. G. Dyall *et al.*, *Comput. Phys. Commun.* **55**, 425 (1989).
- [39] A. M. Costa, M. C. Martins, J. P. Santos, P. Indelicato, and F. Parente, *J. Phys. B* **40**, 57 (2007).
- [40] S. Huotari, K. Hämäläinen, R. Diamant, R. Sharon, C. C. Kao, and M. Deutsch, *Phys. Rev. Lett.* **101**, 043001 (2008).
- [41] T. Schneider, P. L. Chocian, and J. M. Rost, *Phys. Rev. Lett.* **89**, 073002 (2002); T. Schneider and J. M. Rost, *Phys. Rev. A* **67**, 062704 (2003).
- [42] J. L. Campbell, *J. Phys. B* **34**, 3543 (2001).
- [43] M. Polasik, *Phys. Rev. A* **39**, 5092 (1989); M. Polasik, *ibid.* **39**, 616 (1989).
- [44] M. Polasik and M. Lewandowska-Robak, *Phys. Rev. A* **70**, 052502 (2004).
- [45] N. Cue, W. Scholz, and A. Li-Scholz, *Phys. Lett.* **63A**, 54 (1977).
- [46] J. H. Scofield, *At. Data Nucl. Data Tables* **14**, 121 (1974).
- [47] L. Natarajan, *Phys. Rev. A* **78**, 052505 (2008).
- [48] J. Hozzowska, A. K. Kheifets, J.-Cl. Dousse, M. Berset, I. Bray, W. Cao, K. Fennane, Y. Kayser, M. Kavčič, J. Szlachetko, and M. Szlachetko, *Phys. Rev. Lett.* **102**, 073006 (2009).